

# The galaxy population of intermediate-redshift clusters

Tomas Dahlén<sup>★</sup>, Claes Fransson, Göran Östlin & Magnus Näslund

*Stockholm Observatory, Stockholm University, SE-106 91 Stockholm, Sweden*

Accepted 2004 January 16. Received 2004 January 15; in original from 2002 June 19

## ABSTRACT

Using photometric redshifts we determine the galaxy population of the clusters of galaxies Cl0016+16 at  $z = 0.55$ , Cl1600+41 at  $z = 0.54$ , Cl1601+42 at  $z = 0.54$  and MS1008–1224 at  $z = 0.31$ . Comparing the clusters, we find no evidence for a universal shape of the total luminosity function (LF) at these redshifts. When dividing the LFs into spectral types, we find that the LF of the early-type galaxies alone can be described by a Gaussian, while the LF of the late-type galaxies is well fitted by a Schechter function, suggesting that the separate LFs for different populations may be universal. The difference in the total LFs can mainly be attributed to the varying relative normalisation of these populations, implying that clusters with an abundant population of late-type galaxies also have steeper faint-end slopes. In MS1008–1224 we detect a faint blue population that dominates over a population with colours consistent with dwarf ellipticals, opposite to clusters at lower redshift.

Compared to low-redshift clusters, we find that a general fading of the late-type population by  $\sim 2$  mag and the early-type population by  $\sim 1$  mag describes the evolution from  $z = 0.55$  to  $z = 0$  well.

As a consequence of the different early-type and late-type LFs and their dependence on cluster radius, the fraction of blue cluster galaxies, as measured by the Butcher–Oemler effect, differs between the clusters and depends on limiting magnitude and radius.

We find a correlation between the dwarf-to-giant ratio and the surface density, indicating that the high density environment in the cluster cores is hostile to dwarf galaxies.

**Key words:** galaxies: clusters: general – galaxies: distances and redshifts – galaxies: luminosity function, mass function – cosmology: observations.

## 1 INTRODUCTION

Ever since the results of Butcher & Oemler (1984, hereafter BO84), showing that the fraction of blue galaxies in clusters increases rapidly between  $z = 0$  and  $z \sim 0.5$ , it has been clear that there is strong evolution in cluster galaxy populations with redshift. These results have been confirmed by subsequent surveys (e.g. Rakos & Schombert 1995; Ellingson et al. 2001; Kodama & Bower 2001; Margoniner et al. 2001). A general picture explaining the over-all features of cluster formation and evolution is given within the cold dark matter (CDM) hierarchical clustering scenario (e.g. Bower 1991; Kauffmann & White 1993; Kauffmann 1995; Baugh, Cole & Frenk 1996). A large number of observations and N-body simulations now support this scenario. The bluing with redshift of the cluster galaxies is explained by a

higher accretion rate of star forming field galaxies at higher redshift (Bower 1991), possibly combined with a general increase in star formation in field galaxies at higher  $z$  (Diaferio et al. 2001). A consequence of the CDM model is that high- $z$  clusters assemble during a much shorter time interval than comparably rich clusters today (Kauffmann 1995). This general scenario is also supported by the observed increase of mergers in high-redshift clusters (van Dokkum et al. 1999). Furthermore, N-body simulations (e.g., Dubinski 1998) show that the brightest cluster galaxies (BCG) naturally form via mergers in a hierarchical scenario.

The difference in radial distribution between early-type and late-type galaxies in clusters can be explained by the hierarchical model if infalling field galaxies, which are predominantly blue star-forming galaxies, have their star formation truncated as they fall deeper into the cluster potential (Balogh, Navarro & Morris 2000; Diaferio et al. 2001). Mergers and interactions in the high-density cluster environ-

<sup>★</sup> E-mail: tomas@astro.su.se. Present address: Space Telescope Science Institute, 3700 San Martin Dr., Baltimore, MD 21218

ment also affect the star formation, transforming the spectral type of the galaxies.

One of the most important probes of cluster evolution is the luminosity function (hereafter LF), describing the number of galaxies per magnitude bin in a cluster. Binggeli, Sandage & Tammann (1988) showed that the total LF for the Virgo cluster rises as a Gaussian at bright magnitudes and then flattens to a "plateau" (or even a slight decrease), before it turns steep at faint magnitudes. LFs with similar shapes are found in other nearby clusters, e.g. Coma (Trentham 1998a). The existence of a numerous population of faint dwarf galaxies in clusters, more common than in the field, is verified by a number of observations (e.g., Smith, Driver & Phillipps 1997; Wilson et al. 1997; Phillipps et al. 1998; Trentham 1998a; Yagi et al. 2002). There are, however, also clusters that do not show this steep increase at faint magnitudes (Trentham 1998b, 1998c). Most likely, this is a consequence of different evolution depending on e.g., richness and epoch of formation.

Conselice, Gallagher & Wyse (2001) discuss different scenarios that could lead to the dwarf population in local clusters. By comparing models with the observed kinematic and spatial properties of a number of Virgo cluster galaxies, they suggest that a transformation of spirals into dwarf ellipticals (dEs) by "galaxy harassment" (Moore, Lake & Katz 1998) is occurring. Some dEs may, however, have formed outside the cluster in galaxy groups, which were later accreted. These dEs may therefore be as old as the cluster ellipticals. The fading of these cluster galaxies into todays dwarf population is discussed by Wilson et al. (1997) and Smail et al. (1998).

Besides measuring the total LF, it is of high interest to investigate the LFs of different galaxy populations and their evolution with redshift. While previous studies of type-dependent LFs have focused on *morphological types*, e.g., Binggeli et al. (1988) and Andreon (1998), here we divide galaxies into *spectral types* characterised by their colours, as described in Section 3.3. In this paper, when we refer to galaxies as early-types and late-types we mean their spectral type, while morphological types are denoted by their type in the Hubble sequence, e.g., ellipticals and spirals.

A consequence of the hierarchical scenario is that clusters observed at high redshift ( $z \gtrsim 0.5$ ), where the infall of field galaxies is assumed to peak (Bower, Kodama & Terlevich 1998), should have a higher fraction of late-type galaxies compared to local clusters. This should lead to a differential evolution between the late-type and early-type cluster LFs with redshift, with the late-type LF shifted towards brighter magnitudes at increasing redshift, as compared to the early-types.

Because it is observationally costly, if at all possible, to obtain redshifts for the numerous faint population, most observational efforts to study galaxy populations in high- $z$  clusters have concentrated on the brighter galaxies ( $M_B \lesssim -19$ ). Recently, however, photometric redshifts have been demonstrated to be a powerful tool for studying especially the faint population of cluster galaxies. Even though the accuracy of photometric redshifts can not be compared to spectroscopic redshifts, they can provide a reliable determination of clusters membership, and therefore significantly reduce the necessary amount of field galaxy subtraction. In a previous paper (Dahlén, Fransson & Näslund 2002, here-

after DFN02), we demonstrated the use of photometric redshifts in a study of the population of the intermediate rich cluster Cl1601+42 at  $z = 0.54$ . The photometric redshift selection minimizes the amount of background subtraction needed. Internal properties of the cluster, such as radial distribution and luminosity function, both for the total cluster population, as well as for different populations separately, can therefore be determined. Here we extend our previous study of Cl1601+42 to include two additional rich clusters, Cl0016+16 at  $z = 0.55$  and MS1008-1224 at  $z = 0.31$ . We also include observations of a fourth poor cluster, Cl1600+41 at  $z = 0.54$ .

Throughout this paper we assume a Hubble constant  $H_0 = 50 \text{ km s}^{-1} \text{ Mpc}^{-1}$ , and a cosmology with  $\Omega_M = 0.3$  and  $\Omega_\Lambda = 0.7$ , unless anything else is assumed. Magnitudes are given in the Vega based system.

## 2 THE DATA

### 2.1 Observations

The positions of the four clusters and a blank field, used for background subtraction, are listed in Table 1. All observations, except those of MS1008-1224, were carried out with the 2.56-m Nordic Optical Telescope (NOT) and the Andalucia Faint Object Spectrograph and Camera (ALFOSC) during six observing runs between 1997 and 2001. The clusters and the background field were observed in four filters,  $B$ ,  $V$ ,  $R$  and  $I$ , and additional observations in the  $U$  filter were obtained for Cl1601+42. Observations were performed under photometric conditions. The seeing in the images varies between  $0''.70$  and  $1''.15$ . A complete log of the observations is given in Table 2.

The observations of MS1008-1224 were carried out by the Science Verification Team at ESO using FORS at the VLT. The cluster was observed in  $B, V, R, I$  FORS Bessel filters with exposure times  $\sim 1 - 1.5\text{h}$ . The images were reduced using the IRAF package. The seeing in the final coadded frames is  $(0''.72, 0''.65, 0''.64, 0''.55)$  in the  $(B, V, R, I)$  filter. Further details can be found at the ESO web site<sup>†</sup>. Information on redshifts, galactic extinction, observed area, X-ray luminosities and velocity dispersion of the clusters is given in Table 3.

### 2.2 Data reductions

The data obtained with the NOT were reduced using the IRAF package. Bias subtraction and flat-fielding were made in a standard manner. For the  $I$ -band we constructed a fringe-frame after removing objects from the science images. The fringe-frame was then subtracted from each science image, scaled to the appropriate background level. The images were corrected for atmospheric extinction, aligned, and finally combined. Calibration was done using standard stars from Landolt (1992). The galaxies were corrected for galactic extinction according to Schlegel, Finkbeiner & Davis (1998). A description of data reduction and calibration of the MS1008-1224 images is given at the ESO web page.

<sup>†</sup> URL <http://www.hq.eso.org/science/ut1sv>

**Table 1.** Positions of the observed clusters and back ground field given in J2000 coordinates.

Object	RA	Dec
Cl0016+16	00 <sup>h</sup> 18 <sup>m</sup> 33 <sup>s</sup> .3	16° 26' 36"
Cl1600+41	16 <sup>h</sup> 02 <sup>m</sup> 06 <sup>s</sup> .1	41° 01' 23"
Cl1601+42	16 <sup>h</sup> 03 <sup>m</sup> 09 <sup>s</sup> .8	42° 45' 18"
MS1008-1224	10 <sup>h</sup> 10 <sup>m</sup> 34 <sup>s</sup> .1	-12° 39' 48"
Blank field	16 <sup>h</sup> 08 <sup>m</sup> 54 <sup>s</sup> .0	41° 34' 00"

**Table 2.** Log of observations.

Object	Filter	Obs. date	Exp. time	# of exp.	Seeing	1 $\sigma$ (mag arcsec $^{-2}$ )
Cl0016+16	<i>B</i>	Aug 00	18000s	20	0''.92	27.7
	<i>V</i>	Aug 00	17100s	19	1''.03	27.3
	<i>R</i>	Aug 00	7200s	8	0''.73	26.6
	<i>I</i>	Aug 00	16200s	36	0''.74	26.0
Cl1600+41	<i>B</i>	Jun 01	18000s	20	0''.89	27.8
	<i>V</i>	Jun 01	12600s	14	0''.86	27.2
	<i>R</i>	Jun 01	8100s	9	0''.89	26.7
	<i>I</i>	Jun 01	18000s	30	0''.83	26.2
Cl1601+42	<i>U</i>	Apr/Jun 99	25200s	14	0''.89	26.7
	<i>B</i>	Jun 98	12600s	14	0''.84	27.5
	<i>V</i>	Apr 99	16200s	18	1''.02	27.3
	<i>R</i>	Jun 97	7200s	8	0''.75	26.8
Blank field	<i>I</i>	Jun 98/Jun 99	14400s	24	0''.76	26.2
	<i>B</i>	Aug 00	16200s	18	1''.15	27.6
	<i>V</i>	Jun 99	16200s	18	1''.02	27.0
	<i>R</i>	Jun 97	7200s	8	0''.70	26.8
	<i>I</i>	Aug 00	16200s	36	0''.73	26.8

Photometry was obtained using the FOCAS package (Jarvis & Tyson 1981; Valdes 1982; Valdes 1993). The detection limit was set to  $3\sigma$  of the sky noise, and a minimum detection area corresponding to the seeing-disc was used. For each object and filter, we made a catalogue listing isophotal magnitude, aperture magnitude, position and area. When calculating the aperture magnitude we first smoothed the observations to the seeing of the filter with the worst seeing of each cluster, and then used a constant aperture size with a radius corresponding to this seeing. Finally, a combined catalogue for each object was made by using the positions in the *R*-catalogue and matching these with the positions in the other catalogues.

The completeness was tested with simulations where we added artificial galaxies with different magnitudes and radial profiles to the real images. Using the same detection procedures as for the real data we find that 100 per cent of the galaxies are detected down to  $m_R = 25$  for all our objects. Using simulations we also calculate corrections that should be applied when calculating total magnitudes from the observed isophotal magnitudes. These simulations are described in Näslund, Fransson & Hultgren (2000) and DFN02.

In Table 4 we list the number of objects in each catalogue to a limiting magnitude  $m_R < 25$ . We also list the number of objects having aperture photometry in at least four filters (i.e four or five filters for Cl1601+42, and four filters for the other objects), three filters, as well as in two or one filter only. Objects identified as stars by visual inspection of the psf, are excluded.

### 3 PHOTOMETRIC REDSHIFTS

An extended discussion on the use of photometric redshifts applied to clusters of galaxies is given in DFN02. Here we present a brief summary of the technique. For every object we minimize the expression

$$\chi^2(t, z, m_\alpha) = \sum_i \frac{(m_i - (T_i(t, z) + m_\alpha))^2}{\sigma_i^2} \quad (1)$$

where  $m_i$  and  $\sigma_i$  are the observed magnitudes and uncertainties in filter  $i$ , respectively.  $T_i(t, z)$  is the magnitude in the  $i$ -filter of template  $t$ , redshifted to  $z$ . This magnitude is calculated by convolving the filter curve and the quantum efficiency of the detector with the galaxy template. The quantity  $m_\alpha$  is a constant, which fits the apparent magnitude of the template galaxy.

A set of ten different templates are used. We construct these by interpolations between the four observed galaxy templates given by Coleman, Wu & Weedman (1980). These represent E, Sbc, Scd and Im galaxies. Absorption due to intergalactic H I clouds is treated as in Madau (1995). We also include eight stellar templates of M-dwarfs taken from Gunn & Stryker (1983).

A modification compared to DFN02 is that we here use a "Bayesian" approach (e.g. Kodama, Bell & Bower 1999; Benitez 2000). This method allows the incorporation of pre-existing knowledge about the galaxies into the photometric redshift determination. This is illustrated in Fig. 1, where we in the top panel show the probability distribution derived from the chi-square fit according to Eq.(1), for a galaxy with known spectroscopic redshift  $z = 0.31$ . There are ten local minima in the chi-square fit, resulting in ten probabili-

**Table 3.** Properties of the cluster sample.

Cluster	Redshift	$A_V^a$	Observed area sq. arcmin	Diameter <sup>b</sup> Mpc	$L_x$ (0.3-3.5 keV) $10^{44}$ erg s $^{-1}$	$\sigma$ km s $^{-1}$
Cl0016+16	0.546 <sup>c</sup>	0.19	32.5	3.1	34.7 <sup>d</sup>	1703 <sup>d</sup>
Cl1600+41	0.540 <sup>i</sup>	0.04	28.9	2.9	<2.0 <sup>i,j</sup>	-
Cl1601+42	0.539 <sup>e</sup>	0.03	30.4	3.0	2.1 <sup>d</sup>	1166 <sup>d</sup>
MS1008-1224	0.306 <sup>f</sup>	0.23	32.4	2.2	5.8 <sup>g</sup>	1054 <sup>h</sup>

Notes:

- a) Schlegel et al. 1998
- b) Cluster diameter covered by observations.
- c) Dressler & Gunn 1992
- d) Smail et al. 1997.
- e) Oke, Gunn & Hoessel 1996.
- f) Lewis et al. 1999.
- g) Gioia & Luppino 1994.
- h) Carlberg et al. 1996.
- i) Henry et al. 1982.
- j) Converted from energy band 0.5-4.5 keV assuming electron temperature 4 keV

**Table 4.** Number of objects with  $m_R < 25$  in the different images, and the number of objects with aperture photometry in four to five filters, three filters, and one or two filters only. Stars are excluded.

Image	No. of Objects	$\geq 4$ filters	3 filters	1-2 filters
Cl0016+16	1430	1154	172	104
Cl1600+41	809	791	13	5
Cl1601+42	1199	1034	106	59
MS1008-1224	1665	1544	104	17
Field1	945	781	87	77

ity maxima, divided into two groups, one at low, and one at high redshifts. The best-fitting template is in this case an Sa galaxy with redshift  $z = 0.20$ , but almost as good fits are achieved for the three other templates with  $z < 0.5$ , representing E to Sbc galaxies. There are also maxima with high probability at  $z \sim 2.8 - 3.5$ . The degeneracy of the high- and a low-redshift groups arise because the Lyman-break falls approximately between the same filters at  $z \sim 3.5$ , as the 4000-Å break does at  $z \sim 0.3$ .

The absolute magnitude for this galaxy at  $z \sim 3.5$  would, however, be unrealistic,  $M_B \sim -28$ , whereas at  $z \sim 0.1$  and  $z \sim 0.3$  we get  $M_B \sim -18$  and  $M_B \sim -20.5$ , respectively. To account for this one could weight the probability function with an expected LF, an approach used by Kodama et al. (1999). However, since we are here interested in *determining* the LF, we can not use this method. Instead, we use an exponential cut-off two magnitudes brighter than  $M_B^*$ , where  $M_B^*$  is determined by a fit to the Schechter function without any weighting. The effect of introducing this cut-off at bright magnitudes is mainly to suppress the false peaks introduced by the misidentification between the Lyman-break and the 4000-Å break. An alternative would be to truncate the procedure at e.g.  $z = 2$ . However, at  $m_R \sim 25$ , galaxies at  $z \gtrsim 2$  with "normal" absolute magnitudes are expected; a cut-off could here lead to a misidentification of these galaxies. Furthermore, the volume element increases with redshift (up to  $z \sim 1.8$ , dotted line in the top panel of Fig. 1). Therefore, of two maxima with the same probability from the chi-square fit, the higher redshift should for constant comoving density, be more likely due to the larger volume.

The lower panel of Fig. 1 shows the probability distribution for the same galaxy after multiplying the result from the top panel with the probability distribution derived after applying an exponential cut-off at bright magnitudes and a weighting by the volume element. The distributions are normalised to unit area.

The peaks at  $z > 2.5$  have now disappeared, and the lowest redshift peaks are suppressed due to the smaller volume element. The maximum probability is now for a Sb galaxy at  $z = 0.31$ , which matches the spectroscopic redshift.

The "Bayesian" approach we use mostly affects the determination of redshifts for the cluster MS1008-1224 at  $z = 0.31$ . Liu & Green (1998) show that when using photometric redshifts there is a risk of misidentification between Sbc galaxies at  $z \sim 0.05$  and Scd/Im galaxies at  $z \sim 0.3$ . From our example above we also note that  $\sim$  Sb galaxies at  $z \sim 0.3$  can be misidentified as E galaxies at  $z \lesssim 0.1$ .

When estimating the dispersion between spectroscopic and photometric redshifts for 61 galaxies in the field of MS1008-1224, we find  $\sigma_z \sim 0.051$ , when we use the "Bayesian" approach, compared to  $\sigma_z \sim 0.11$  without it. The increased dispersion is mainly due to a few galaxies achieving large errors. Excluding six galaxies reduces the dispersion to  $\sigma_z \sim 0.058$ . For the clusters at  $z \sim 0.55$  the effect of including this weighting is marginal. Here we get  $\sigma_z \sim 0.054$  with the "Bayesian" approach and  $\sigma_z \sim 0.060$  without, when calculating the dispersion between the photometric and spectroscopic redshifts for 38 galaxies in the field containing Cl0016+16.

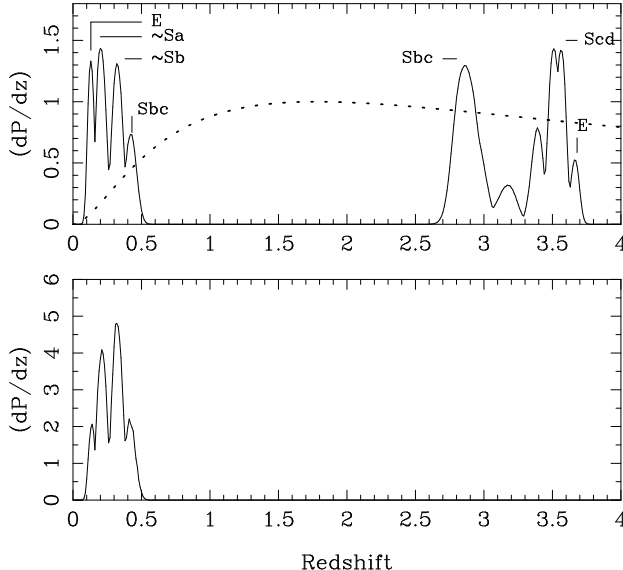


**Figure 1.** Chi-square probability function for the template fitting method, for a galaxy with known spectroscopic redshift  $z = 0.31$ . At each redshift the probability of the galaxy template that has the minimum chi-square, i.e. the highest probability is plotted. The top panel shows the probability function without considering absolute magnitudes or volume element. The dotted line shows the redshift dependence of the volume element. In the bottom panel we use a cut-off at bright magnitudes, and take the volume element into account. For some of the peaks we plot the associated galaxy type. The distributions are normalised to unit area.

The example shown in Fig. 1 was picked to illustrate the "Bayesian" method, and has an unusual high number of probability peaks with similar strengths. Most galaxies have a more clearly defined primary peak.

Possible systematic effects when using photometric redshifts are discussed in DFN02. In summary, we find a marginal increase in the photometric redshift errors for the faintest galaxies ( $m_R \gtrsim 24$ ) due to increased photometric errors. These errors mostly affect late type galaxies. In numbers, we find a possible increase in redshift uncertainty by  $\Delta\sigma_z \sim 0.01$  due to systematic effects at  $m_R \gtrsim 24$ . This may lead to an underestimate of the number of cluster galaxies in the faintest bins by  $\sim 5\%$ . This result shows that systematic errors are unlikely to dominate over statistical errors.

### 3.1 Photometric redshift catalogue

We calculate photometric redshifts for all objects with  $m_R \leq 25$  and aperture photometry in at least three filters, which corresponds to 92–99 per cent of the total number of objects to this limit (Table 4). The accuracy of the photometric redshifts is estimated by comparing our result with available spectroscopic redshifts. In Table 5 we list the number of available redshifts and the rms deviation between the photometric and spectroscopic redshifts,  $\sigma_z$ . The galaxies used for calculating the rms have photometry in all filters. To estimate the increase in errors for objects only having photometry in three filters, we also calculate the rms deviation after excluding the filter with the largest error for each galaxy,  $\sigma_z^{(3)}$ .

### 3.2 Comment on background counts

To estimate the background contamination we use *BVRI* photometry of our blank field. In DFN02 we used *UBVRI* photometry of the ESO Imaging Survey (EIS) deep field published by da Costa et al. (1998). Number counts to  $R = 25$  for Field1 and the EIS field yield  $983 \pm 133$  and  $845 \pm 120$  galaxies, respectively, where the fields are normalised to the same size as the image of Cl0016+16 (32.5 sq. arcmin). Errors represent  $1\sigma$  and include Poisson statistics and field-to-field variance (see DFN02 for a discussion). The resulting counts are therefore consistent within the errors.

When determining the background counts within the cluster redshift range, we find a larger deviation between the two fields. In the redshift range  $z_{Cl0016} \pm 1.5\sigma_z$ , we find  $121 \pm 20$  galaxies for Field1, and  $166 \pm 26$  galaxies for the EIS field to  $R = 25$ . These results are marginally within errors, but it is likely that there are systematic effects responsible for some of the off-set. In particular, the aperture magnitudes are determined differently. For our blank field we smooth the images to the same seeing before calculating the colours, whereas the aperture magnitudes given for the EIS field have a varying seeing in the different bands. This can affect the colours, especially for small objects that do not cover the whole aperture.

To check the effect of this, we calculate photometric redshifts for the field containing Cl0016+16 without smoothing the images to the same seeing. Comparing with the 38 objects that have spectroscopic redshifts we find an rms deviation  $\sigma_z = 0.078$ , which is considerably larger than what we found after smoothing,  $\sigma_z = 0.054$ . Therefore, the photometric redshifts calculated for the EIS catalogue are likely to be less accurate.

Finally, systematic errors could be introduced by the uncertainty in the zero-point magnitudes and the use of different software when doing the photometry, i.e. the use of FOCAS for Field1, and SExtractor for the EIS field.

To minimize the risk of introducing systematic errors, we use the photometry from our blank field in this analysis, since this is derived in the same way as the photometry of the cluster images. The use of a different background field does, however, not affect the result in DFN02 on Cl1601+42 more than marginally, i.e. any differences are within the quoted errors. This illustrates the advantage of the photometric method for examining high- $z$  clusters; the relatively small corrections for background contamination makes the results less dependent on the background.

### 3.3 Cluster membership and galaxy classification

For selecting cluster members we use a redshift range  $\pm 1.5\sigma_z$  around the mean redshift of the cluster, with values of  $\sigma_z$  given in Table 5. To account for the increase in dispersion for the galaxies only detected in three filters (Table 3), we use the corresponding  $\sigma_z^{(3)}$  for these galaxies. Note, however, that the information given by a non-detection (i.e., that the magnitude of the galaxy is fainter than the magnitude limit of the observations) is taken into account in the template fitting procedure. Assuming that the errors are Gaussian, the  $1.5\sigma_z$  cut should include  $\sim 86$  per cent of the actual number of cluster galaxies to our limit. Taking into account the small fraction of the galaxies observed in three filters

**Table 5.** N is the Number of galaxies with spectroscopic redshifts used to determine the dispersion between photometric and spectroscopic redshifts,  $\sigma_z$  is the dispersion using information from all filters, while  $\sigma_z^{(3)}$  is the dispersion using only three filters. Also given is the resulting number of clusters galaxies within  $z_{Cl} \pm 1.5\sigma_z$  for the total areas and inside a common radius of 1 Mpc. We also list the density of background galaxies within each redshift range. The limiting magnitude is  $M_B = -17.7$ , corresponding to  $m_R \sim 25$  at  $z = 0.54$  and  $m_R \sim 23.4$  at  $z = 0.31$ .

Cluster	$z_{Cl}$	N	$\sigma_z$	$\sigma_z^{(3)}$	Cluster galaxies		Background <sup>a</sup> (Mpc <sup>-2</sup> )
					Total area	$R < 1$ Mpc	
Cl0016+16	0.546	38 <sup>b</sup>	0.054	0.080 <sup>c</sup>	463 $\pm$ 32	248 $\pm$ 19	12.7 $\pm$ 2.1
Cl1600+41	0.540	<sup>d</sup>	0.065 <sup>d</sup>	0.10 <sup>d</sup>	36 $\pm$ 24	26 $\pm$ 12	14.6 $\pm$ 2.4
Cl1601+42	0.539	78 <sup>b</sup>	0.076	0.12 <sup>e</sup>	332 $\pm$ 35	154 $\pm$ 18	18.8 $\pm$ 2.9
MS1008-1224	0.306	61 <sup>f</sup>	0.051	0.067	221 $\pm$ 20	173 $\pm$ 16	11.6 $\pm$ 2.3
MS1008-1224 <sup>g</sup>					319 $\pm$ 26	240 $\pm$ 21	20.6 $\pm$ 3.5

Notes:

a) Measured within the redshift range defining the different clusters, i.e.  $z_{Cl} \pm 1.5\sigma_z$ .

b) Dressler et al. 1999.

c) Excluding two outliers with large errors.

d) No spectroscopic redshifts available, except for central galaxy. We assume dispersions equal to the mean of the dispersions of the two clusters at similar redshift.

e) Excluding five outliers.

f) Yee et al. 1998.

g) Number of galaxies to  $M_B = -16.2$ .

only that may result in outliers with large errors, we estimate that we include  $\sim 80 - 85$  per cent of the total number of cluster galaxies when applying the  $1.5\sigma$  cut. For a discussion on completeness and contamination when selecting cluster members using photometric redshift, see Brunner & Lubin (2000).

In this study we divide the galaxies into late-types and early-types, based on the spectral type determined by the photometric colours of the galaxies. The division is made half way between the E and Sbc templates from Coleman et al. (1980), approximately corresponding to a rest-frame colour  $B - V = 0.8$ . The first category consists of early-type galaxies with red colours, which are mostly ellipticals and lenticulars, but also include passive spirals with red colours. The second category includes late-type spirals and irregulars, with a possible inclusion of blue elliptical systems.

## 4 RESULTS

The distribution of photometric redshifts in the cluster fields, after subtracting background galaxies, is shown in the left and middle panels in Fig. 2. The right-hand panel shows the redshift distribution of the background field. The location of the clusters is apparent for all clusters except Cl1600+41. We comment on this cluster in next subsection.

As a measure of the richness of the clusters we give in Table 5 the number of cluster galaxies with  $M_B < -17.7$  for the total areas (see Table 3), as well as inside a common radius of 1 Mpc. We also list the density of background galaxies within the redshift range adopted for the different clusters. For the lower-redshift cluster, MS1008-1224, we also give numbers for  $M_B < -16.2$ .

In the left-hand panel of Fig. 3, we show the surface density of galaxies with  $M_B < -17.7$  for the four clusters as a function of radius. The horizontal solid line marks the surface density of the background field in the redshift range of Cl1600+41. Error bars and dashed lines represent  $1\sigma$  errors. The right-hand panel of Fig. 3 shows the projected fraction of early-type galaxies for the four clusters. The hor-

izontal line marks the early-type fraction of the background field at  $z \sim 0.55$ , which is also similar to what we find at  $z \sim 0.31$ . All clusters have an early-type fraction clearly above the field value in the core region. In Cl0016+16 this fraction is  $\sim 85$  per cent in the core. This decreases with radius, but stays above 50 per cent for the whole area covered. The early-type fractions in Cl1601+42 and MS1008-1224 is  $\sim 60$  per cent in the core, and show a decrease which approaches the field value at large radius, even though the deviation from the field is still significant at the outermost points. For Cl1600+41, only the innermost point has a late type fraction deviating from the field. From both figures it is clear that we do not reach the field in any of the clusters, except Cl1600+41.

In Fig. 4, we show the observed colour-magnitude (CM) diagram for all galaxies within the cluster redshift ranges for the three rich clusters, with different symbols representing early-type and late-type galaxies. At the redshifts of the clusters, the plotted colours approximately represent rest-frame  $B - V$ . From the figure, it is evident that the early-type galaxies populate a fairly narrow sequence in the CM diagram, which is clearly redder than the late-type galaxies. Also, the relative fraction of early-type galaxies decreases at fainter magnitudes. Note, however, that the spectral type is not independent of e.g., the rest-frame  $B - V$  colour, since colours are used when determining the photometric redshift, as well as spectral type.

### 4.1 The poor cluster Cl1600+41

From the results above it is clear that Cl1600+41 is very poor, with only  $36 \pm 24$  cluster galaxies with  $m_R < 25$ . Fig. 3 also indicates that if at all significant, the radial extent of the cluster is less than  $\sim 0.5$  Mpc. At larger radii the surface density is marginally below the field value, while the late type fraction is consistent with the late type fraction of the field.

The most significant indication of a cluster comes from the colour distribution, where the innermost point shows a

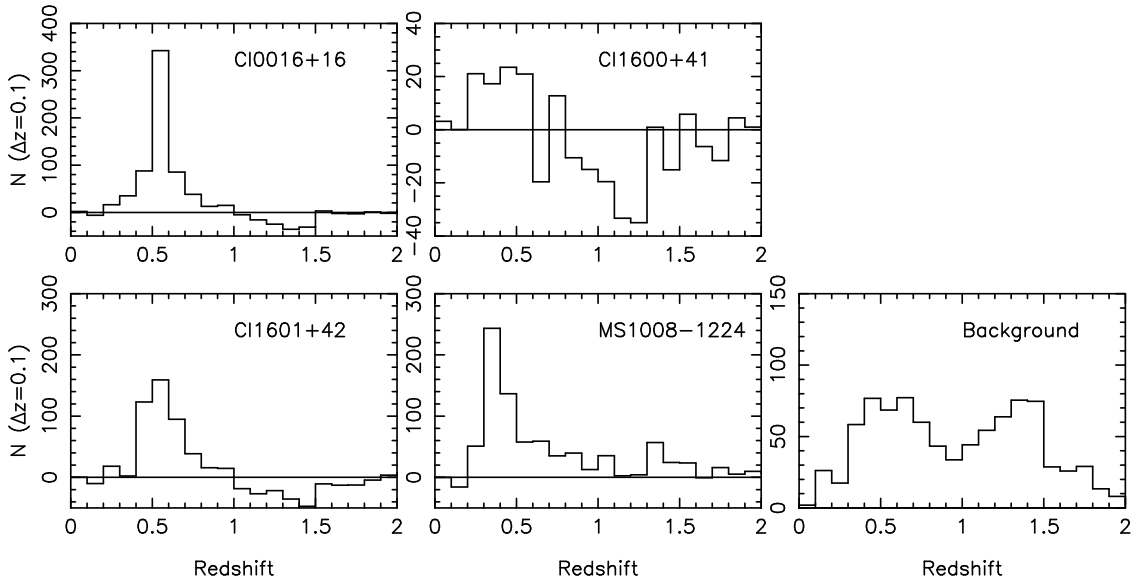


**Figure 2.** The left and the middle panels show the distribution of photometric redshifts in the cluster images after subtracting background galaxies. The right-hand panel shows the redshift distribution of the background field. Note the different scales on the  $y$ -axis. The peak in the background distribution at  $z \sim 1.4$  is most likely caused by the lack of infrared photometry. All distributions above  $z \sim 1$  should therefore be viewed by caution.

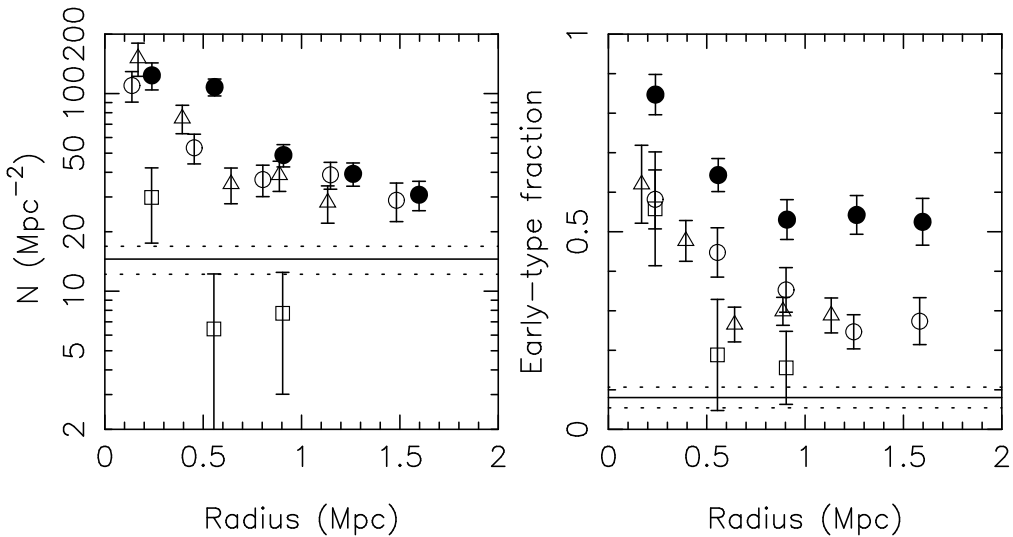


**Figure 4.** Left-hand panel: Projected surface density as function of radius for Cl0016+16 (filled circles), Cl1600+41 (squares), Cl1601+42 (open circles) and MS1008-1224 (triangles). The horizontal line shows the surface density of the background field in the redshift range of Cl1600+41. Right-hand panel: Early-type fraction as function of radius for the four clusters. The horizontal line shows the early-type fraction of the field at  $z = 0.54$ . The limiting magnitude is  $M_B = -17.7$ . Error bars and the dashed lines represent  $1\sigma$  errors.

clear excess of red galaxies (Fig. 3, right-hand panel). Also, the magnitude and colour of the central galaxy is similar to the brightest cluster galaxy (BCG) in the other clusters. Furthermore, a visual inspection of a three-colour image of Cl1600+41 shows this bright red central galaxy to be surrounded by a number of red and blue galaxies, clearly indicating the presence of a cluster.

If we calculate the number of cluster galaxies in Cl1600+41 by the standard method of subtracting galaxies in a blank field from the cluster image in a *single* band, we get a total of  $9 \pm 127$  cluster galaxies to  $m_R < 25$ . The large error is due to field-to-field variations, which dominate

in the subtraction method. It is obvious that the subtraction method would not result in any cluster detection when using our blank field as a reference for the background counts.

With only 36 selected cluster members within the chosen redshift range, the background counts dominate over the cluster galaxies, i.e. only 22 per cent of the galaxies are expected to be cluster galaxies, as compared to 78, 66 and 80 per cent, for Cl0016+16, Cl1601+42 and MS1008-1224. It is clear that this cluster is close to the detection limit. The large contamination in Cl1600+41 makes it impossible to determine either the internal properties of the cluster with any significance, or the cluster LF. Therefore, we do not in-

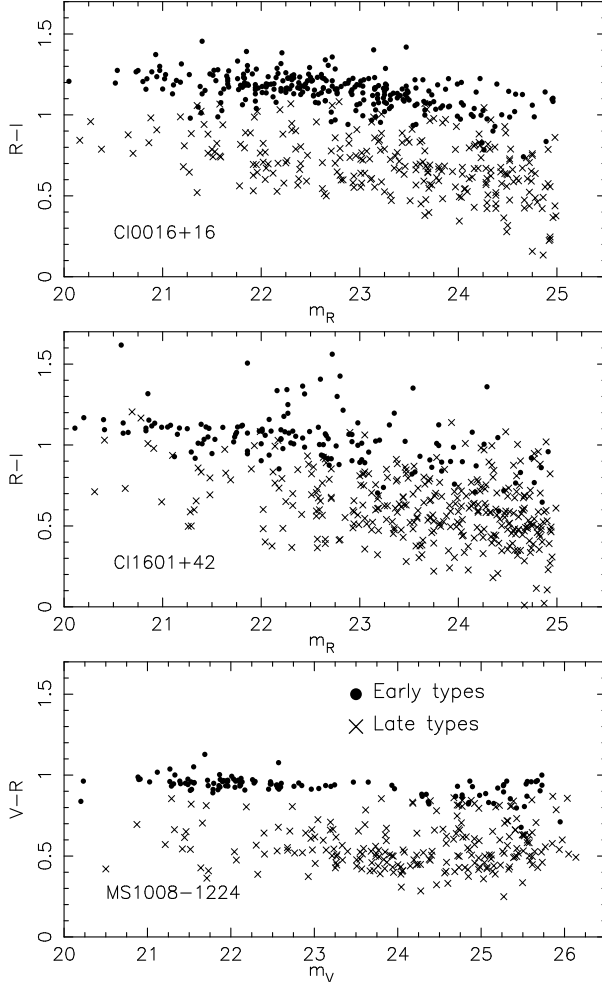


**Figure 3.** Observed colour-magnitude diagrams for Cl0016+16 (top), Cl1601+42 (middle) and MS1008-1224 (bottom). Galaxies are separated into early-types and late-types. At the redshifts of the clusters, the observed colours approximately match rest-frame  $B - V$  colour.

clude Cl1600+41 when comparing the LF and the Butcher–Oemler (BO) effect between the clusters.

#### 4.2 The cluster luminosity functions

When calculating the LF we divide the galaxies within the cluster redshift range into magnitude bins with  $\Delta m = 0.5$  to  $M_B = -17.7$  for the two clusters at  $z \sim 0.55$ , and to  $M_B = -16.2$  for MS1008-1224 at  $z \sim 0.31$ . K-corrections are determined for each galaxy using the best-fitting template from the photometric redshift calculations. For each magnitude bin we subtract background galaxies within the redshift range of the different clusters.

The left-hand panels in Fig. 5 show the resulting LFs for the three clusters. As a first step we fit the total LFs to the usual Schechter function (Schechter 1976),

$$\Phi(M) \propto e^{-10^{0.4(M^* - M)}} 10^{-0.4(\alpha+1)M}, \quad (2)$$

where  $M^*$  is the characteristic magnitude, representing the turnoff at the bright end of the LF profile, and  $\alpha$  is the slope at the faint end of the LF. As an alternative to  $\alpha$ , we also

calculate the slope of a straight line fit to the five faintest bins in each LF, according to

$$\Phi_f(M) \propto 10^{-0.4(\alpha_f+1)M} \quad (3)$$

(Trentham 1998a; DFN02). The parameter  $\alpha_f$  gives a better representation of the faint-end of the LF, since it is not affected by the coupling between  $M^*$  and  $\alpha$  in the Schechter function. In Table 6 we list  $M^*$ ,  $\alpha$  and  $\alpha_f$  for the clusters. Parameters are given both for the total cluster populations, and for the late-type population in each cluster.

Fig. 5 shows that the shapes of the LFs of the three clusters differ substantially. To further understand these differences, we plot the LFs divided into early-type and late-type galaxies separately in the right-hand panels of Fig. 5. For all three clusters, the early-type galaxies with  $M_B \lesssim -18$  have a Gaussian LF, peaking at  $M_B^G \sim -20$  (Table 6). We note that the faint early-type population in MS1008-1224 shows an increase below  $M_B = -18$ . We return to this point in Section 5.

The late-type galaxies are better fitted by Schechter functions. However, the relative normalisations of the early-type and late-type LFs vary between the different clusters. In Section 5 we discuss these differences further.

#### 4.3 The Butcher–Oemler effect

We calculate the blue fraction,  $f_B$ , using the definition in BO84. For each cluster we select galaxies with  $M_V < -20$  within a circular radius,  $R_{30}$ , containing 30 per cent of the cluster galaxies. Now,  $f_B$  is the fraction of these galaxies that are at least 0.2 mag bluer than the colour-magnitude relation for the cluster. To account for cluster galaxies outside our field-of-view, we fit the cluster radial profile with a singular isothermal sphere when calculating  $R_{30}$ .

In order to compare results, we adopt in this section only the cosmology used by BO84 ( $q_0 = 0.1$ ). The difference from BO84 is that we here select cluster members with the photometric redshift method. This increases the accuracy since background subtraction is reduced. The blue fractions derived are given in Table 7.

For MS1008-1224, we find a value of  $f_B$  that matches the straight-line fit of the blue fraction as a function of redshift presented in BO84. For Cl1601+42 and Cl0016+16 the values of  $f_B$  are located below this fit. The scatter in the fit is, however, large, and at least for Cl1601+42 this deviation is hardly significant. Cl0016+16 is included in the BO84 sample, and they also note that this cluster is exceptional in the sense that it has a fraction of blue galaxies that is more similar to local clusters than to clusters at  $z > 0.3$ . The blue fraction found by BO84 is  $f_B = 0.02 \pm 0.07$ , which is consistent with our estimate.

#### 4.4 Brightest cluster galaxies

In Table 7 we list the absolute  $B$  magnitude and rest-frame  $B - V$  colour for the brightest cluster galaxy (BCG) in the observed clusters, including the poor cluster Cl1600+41. Even though our sample is small, the results are consistent with the magnitude of the BCG being independent of the richness of the cluster, as shown by e.g. Sandage (1976) and Postman & Lauer (1995). In particular, we note that

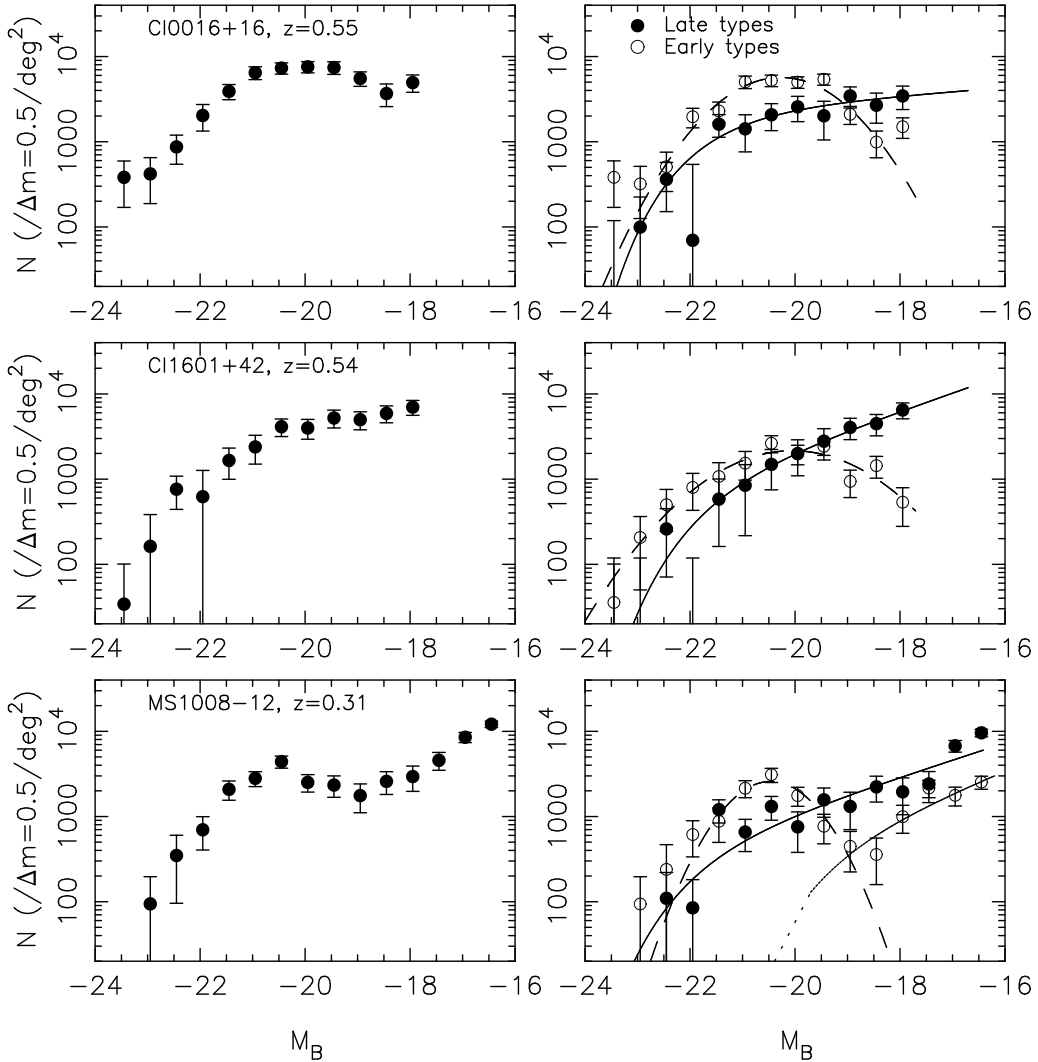


**Figure 5.** Luminosity functions in the rest-frame  $B$ -band for Cl0016+16, Cl1601+42 and MS1008-1224. The left-hand panels show the total LFs, while in the right-hand panels the LFs are divided into early-type (open circles) and late-type (filled circles) galaxies. Error-bars include Poissonian uncertainties and field-to-field variance. For MS1008-1224 we show separate Schechter fits for the early-type and late-type populations.

**Table 6.** Characteristic magnitude,  $M_B^*$  and faint-end slope,  $\alpha$  derived from the Schechter function fit to the rest-frame  $B$ -band LFs for the total population and for late-type galaxies only.  $\alpha_f$  is the slope of a straight-line fit to the five faintest-magnitude bins in each cluster. Limiting magnitude is  $M_B = -17.7$ . For MS1008-1224, we also give results to  $M_B = -16.2$ . For the early-type population,  $M_B^G$  is the peak magnitude and  $\sigma^G$  is the width of a Gaussian fit to  $M_B \leq -18.0$ .

Cluster	All galaxies				Late-types				Early-types			
	$M_B^*$	$\alpha$	$\alpha_f$	$M_B^*$	$\alpha$	$\alpha_f$	$M_B^G$	$\sigma^G$				
Cl0016+16	$-21.07 \pm 0.24$	$-0.55 \pm 0.10$	$-0.65 \pm 0.10$	$-21.75 \pm 0.50$	$-1.12 \pm 0.17$	$-1.17 \pm 0.18$	$-20.27 \pm 0.08$	$1.01 \pm 0.05$				
Cl1601+42	$-21.87 \pm 0.36$	$-1.25 \pm 0.10$	$-1.33 \pm 0.14$	$-21.80 \pm 0.53$	$-1.53 \pm 0.27$	$-1.65 \pm 0.19$	$-20.05 \pm 0.17$	$1.30 \pm 0.10$				
MS1008-1224	$-21.06 \pm 0.17$	$-0.72 \pm 0.26$	$-0.99 \pm 0.15$	$-21.05 \pm 0.58$	$-1.11 \pm 0.33$	$-1.61 \pm 0.24$	$-20.46 \pm 0.10$	$0.73 \pm 0.06$				
MS1008-1224 <sup>a</sup>	$-21.48 \pm 0.17$	$-1.46 \pm 0.09$	$-1.92 \pm 0.13$	$-22.00 \pm 0.37$	$-1.50 \pm 0.17$	$-1.89 \pm 0.16$						

Note:

a) Limiting magnitude  $M_B = -16.2$ .

the BCG of the extremely poor cluster Cl1600+41 is only marginally fainter than the rest, demonstrating that even in this environment a luminous elliptical can be formed.

## 5 DISCUSSION

### 5.1 Variations in the cluster luminosity function

The different shapes of the LFs in our sample suggest that there is no universal form of the total cluster LF at  $z \gtrsim 0.3$

**Table 7.** The blue fraction,  $f_B$ , as defined by BO84, the absolute  $B$  magnitudes and rest-frame  $B - V$  colour for the brightest cluster galaxy in our cluster sample and the early-type fraction at two limiting magnitudes.

Cluster	$z$	$f_B$	$M_B$	$B - V$
Cl0016+16	0.546	0.04 $\pm$ 0.02	-23.52 $\pm$ 0.02	1.00 $\pm$ 0.03
Cl1600+41	0.540	-	-23.36 $\pm$ 0.03	0.92 $\pm$ 0.05
Cl1601+42	0.539	0.15 $\pm$ 0.06	-23.50 $\pm$ 0.04	0.93 $\pm$ 0.07
MS1008-1224	0.306	0.13 $\pm$ 0.06	-23.65 $\pm$ 0.05	1.15 $\pm$ 0.07

(Fig. 5). To quantify this we construct an average LF from the three individual best-fitting LFs. We then calculate the reduced chi-square when fitting each LF to the average LF. We also calculate the reduced chi-square when fitting the individual LFs to a Gaussian+Schechter function. Results are shown in Table 8. The chi-squares are significantly higher for the fits to the average LF, supporting our claim for a non-universal LF. We also find that a single Schechter function gives a poor representation of the cluster LF, which agrees with e.g. Driver et al. (1994) and Wilson et al. (1997). This is especially evident for MS1008-1224, where the best Schechter fit to  $M_B < -17.7$  yields a faint-end slope that is decreasing, while the data-points clearly show an increase in the number of faint galaxies with  $M_B > -19$ . As in the case for Virgo, a better representation is given by the sum of a Gaussian and Schechter function. The reduced chi-square for a Gaussian+Schechter function is  $\chi^2/\nu = 0.98$ , while a single Schechter function yields  $\chi^2/\nu = 5.8$ .

From the separate late-type and early-type LFs (right-hand panels of Fig. 5), it is clear that the relative abundance of the early-type and the late-type populations determines the over-all shape of the LF. In Cl1601+42 late-type galaxies dominate at  $M_B \gtrsim -20$ . This results in a total LF that increases over the whole magnitude range, and has a steep faint-end slope. MS1008-1224 is similar to Cl1601+42 in that it contains a numerous population of faint late-type galaxies, which dominates the total LF at faint magnitudes. The magnitude where this cross-over takes place is, however, slightly fainter in MS1008-1224 ( $M_B \sim -19.5$ ) compared to Cl1601+42 ( $M_B \sim -20$ ), which leads to a total LF where both an intermediate-magnitude Gaussian part, as well as a steep faint-end slope of late-type galaxies are distinguishable. Note also that MS1008-1224 has a population of faint *early-type* galaxies, which adds to this.

In Cl0016+16 there are relatively few faint late-type galaxies, compared to the number of early-type galaxies at  $-21 \lesssim M_B \lesssim -19$ . This leads to a total LF that has a Gaussian shape at intermediate magnitudes, and only at the faintest bin is there an indication of a rise.

As discussed in DFN02, the differences between the shapes of the cluster LFs can be explained by the fact that clusters in the hierarchical clustering scenario at high redshift have a larger fraction of newly accreted galaxies with ongoing star formation. A general increase in the star-formation rate in field galaxies with redshift (Diaferio et al. 2001), also contributes to an increase of star-forming galaxies in clusters at high  $z$ .

After accretion, and a possible period of enhanced star formation, the galaxies could have their gaseous envelopes removed by tides or ram pressure stripping, leading to a fading over time-scales of Gyrs, as the remaining gas reservoir is exhausted ('strangulation') (Balogh et al. 2000; Diaferio et al. 2001). Such fading of the faint blue galaxies is discussed

**Table 8.** Reduced chi-squares when comparing the LFs of Cl0016+16, Cl1601+42 and MS1008-1224 to the best-fitting Gaussian+Schechter function, as well as an LF which is an average of the three individual LFs.

Cluster	$\chi^2/\nu$ (individual fit)	$\chi^2/\nu$ (average fit)
Cl0016+16	0.45	1.25
Cl1601+42	0.46	1.49
MS1008-1224	0.98	1.46

by Wilson et al. (1997), who find that a fading of dwarf irregulars by  $\sim 3$  mag can explain the difference between the LF in clusters  $z \sim 0.2$  and the local Virgo cluster. Further, Conselice et al. (2001) show that spirals accreted at high  $z$  can be transformed into the faint dE population seen in local clusters by "galaxy harassment" (Moore et al. 1998).

It is of obvious interest to compare the LFs of the different populations of these clusters with those of nearby clusters like Coma and Virgo. We then have the paradoxical situation that studies of nearby cluster are limited to one, two or at most three colours, or alternatively to a morphological separation of different classes. A direct comparison with our spectral classification is therefore difficult. As a first step we therefore compare the *total* LF of our clusters with that of Coma at  $z = 0.02$  (Trentham 1998a) and Virgo  $z = 0.003$  (Trentham & Hodgkin 2002).

In Fig. 6 we plot the rest-frame  $B$ -band LF for Cl1601+42 (open circles), Cl0016+16 (filled circles), and MS1008-1224 (triangles) together with the LF for the rich Coma cluster (squares) and the poor Virgo cluster (diamonds). For clarity, the LFs have arbitrary off-sets in the  $y$ -direction. As suggested by our discussion of the individual LFs, we represent the total LF as a sum of a Gaussian and a Schechter function. Because the bright and faint populations have distinctly different properties, we discuss them below separately.

### 5.1.1 The bright population

For Coma the Gaussian peaks at  $M_B^G = -19.3 \pm 0.1$ , indicating a fading of the bright population by  $\Delta M \sim 1$  mag, compared to the high-redshift clusters (Table 6). The total LF of the Virgo cluster only has a marginal Gaussian peak. However, the population of morphologically classified elliptical galaxies, as well as giant spirals, has a clear Gaussian shape peaking at  $M_B^G \sim -19$  (Binggeli et al. 1988; Ferguson & Sandage 1991), supporting a fading of this population similar to that suggested for Coma.

These results are consistent with Smail et al. (1997), who find that the characteristic magnitude  $M_V^*$  for early-type galaxies fade by  $\Delta M \sim 0.7$  mag between  $z = 0.54$  and  $z = 0$ . (We have here converted the results in Smail et al. to our adopted cosmology.) Smail et al. find a weaker

trend for bright late-type galaxies, which fade by  $\Delta M \lesssim 0.4$  mag. An evolution is also found by Kodama & Bower (2001), who estimate that the bright blue galaxy population fades by  $\Delta M \sim 1$  mag between  $z \sim 0.4$  and  $z = 0$ . De Propris et al. (1999) investigate the  $K$ -band luminosity evolution of the bright galaxy population in clusters at  $0.1 < z < 1$ , and find that  $K^*(z)$  is consistent with passive luminosity evolution. We have compared our luminosity evolution with stellar synthesis models from Bruzual & Charlot (2003). We model the Gaussian population with an early-type population characterized by a single burst stellar population of age 8.0 Gyr and a Salpeter IMF. This combination results in colours that match the early-type spectral energy distribution in Coleman et al. (1980). For passive evolution, we find that this population should fade by  $\sim 0.7$  mag since  $z \sim 0.55$ . This is slightly less than the  $\sim 1$  mag evolution that our results suggests. This difference will diminish if we either assume a Scalo IMF, or that the Gaussian population includes a fraction of galaxies with residual star formation.

### 5.1.2 The faint population

In DFN02 we argued that the different shapes of the LF at  $M_B \gtrsim -20$  between Coma and Cl1601+42 can be understood as a result of the dynamically younger age of the latter cluster. The steep blue end of the LF in this cluster should then consist of recently accreted field galaxies, which is supported by the fact that this part of the LF is almost exclusively made up of late-type galaxies. The rapidly increasing fraction of late-type galaxies in the outer parts of the cluster is consistent with this accretion scenario, and is also reflected in the rising blue fraction at large radii in this cluster, as shown in Section 5.4. A fading of the blue star forming galaxies in Cl1601+42 by  $\sim 2$  mag, would transform the LF of Cl1601+42 into a LF similar to Coma.

The steepening of the faint-end in MS1008-1224 is clearly shown in Fig. 6. The slope is somewhat steeper than for Coma, and is shifted towards brighter magnitudes. From Fig. 5 we see that the faint-end of MS1008-1224 is made up of both blue and red galaxies. The slope of the faint blue population is similar to the blue population in Cl1601+42, and a fading by  $\sim 1$  mag of this population would result in a LF similar to the one in MS1008-1224. A subsequent fading by an additional magnitude will make both Cl1601+42 and MS1008-1224 similar to Coma. The fading of the late-type population between  $z = 0.5$  and  $z = 0$  for these two clusters could therefore be described by a relation  $\Delta m \simeq -4z$  mag.

### 5.1.3 The red cluster Cl0016+16

The LF of Cl0016+16 at  $z = 0.55$  differs clearly from Cl1601+42 at the same redshift. The LF of the former is similar to Coma in the plateau region, having a Gaussian shape, but shifted to brighter magnitudes by  $\sim 1$  mag. From Fig. 5 we see that the relatively low abundance of late-type galaxies in Cl0016+16, as compared to Cl1601+42, is responsible for the different shapes of the LF at intermediate magnitudes.

Previous investigations of Cl0016+16 show that the bright galaxy population is dominated by red early-type

galaxies. Koo (1981) found that this cluster has an unusually high fraction of red galaxies compared to other high-redshift clusters, and suggested that the star formation must have ended a few Gyrs before the observed epoch. From the absence of blue galaxies and the small scatter in the colours of the red population, Smail et al. (1995) conclude that the cluster is old, despite its high redshift. Of the ten clusters in the MORPHS sample (Smail et al. 1997) with morphological classification from HST in the redshift range  $0.37 < z < 0.56$ , Cl0016+16 has the lowest fraction of spiral galaxies,  $f_{sp} = 21$  per cent, compared to a mean of  $f_{sp} = 44 \pm 7$  per cent for the remaining nine clusters.

The low spiral fraction is, not unexpectedly, related to the low blue fraction found in Cl0016+16, which indicates that the cluster does not follow the general blueing described by the BO-effect. This may be explained by a higher dynamical age for Cl0016+16, which is supported by the high X-ray luminosity and velocity dispersion (Table 3), indicating that Cl0016+16 is more relaxed than Cl1601+42.

Cl0016+16 has a very high fraction of post-starburst galaxies. These galaxies have no current star formation, but were forming stars  $\sim 1$ –2 Gyr before we observe them. Poggianti et al. (1999) found that  $32 \pm 9$  per cent of the galaxies brighter than  $M_V \sim -20.5$  in Cl0016+16 are spectroscopically consistent with this type of galaxies. This suggests that a large fraction of the galaxies in Cl0016+16 has experienced star formation since  $z \sim 0.8$ , but have subsequently faded to become red at  $z = 0.54$ . Post-starburst galaxies are less frequent in local clusters (Poggianti et al. 1999), and although not actively forming stars, Cl0016+16 is therefore not similar to a local cluster placed at high redshift. This is also supported by the brighter early-type population in this cluster compared to local clusters.

The difference between rich clusters at high and low redshift can qualitatively be explained within the hierarchical clustering scenario. Kauffmann (1995) shows that high- $z$  rich clusters assemble over a shorter time interval than low- $z$  clusters of similar richness. In general, this naturally leads to a higher fraction of blue galaxies in high- $z$  clusters. The properties of Cl0016+16 can then be understood if it formed during a short time interval at  $z \gtrsim 0.8$ , leaving a high fraction of post-starburst galaxies. This suggests that the cluster was blue at  $z \sim 0.8$ , while the red colours at  $z = 0.55$  indicates a very low infall of field galaxies during the last  $\sim 1$  Gyr before it is observed.

It is possible that the special environment of Cl0016+16 could have an influence on the blue fraction and the cluster LF. Connolly et al. (1996) and Hughes & Birkinshaw (1998) provide strong evidence that Cl0016+16 is part of a supercluster structure, with two associated clusters at similar redshift with projected distances of 5 and 13 Mpc. The formation of this giant structure could have depleted the number of field galaxies surrounding Cl0016+16, and therefore the accretion rate of late type galaxies.

### 5.1.4 A universal cluster LF?

To summarise our discussion, we find no evidence for a universal shape of the total cluster LF, in agreement with e.g., Binggeli et al. (1988) and Driver, Couch & Phillipps (1998). The LFs for the spectroscopic early-type and late-type galaxies separately have, however, similar shape in the

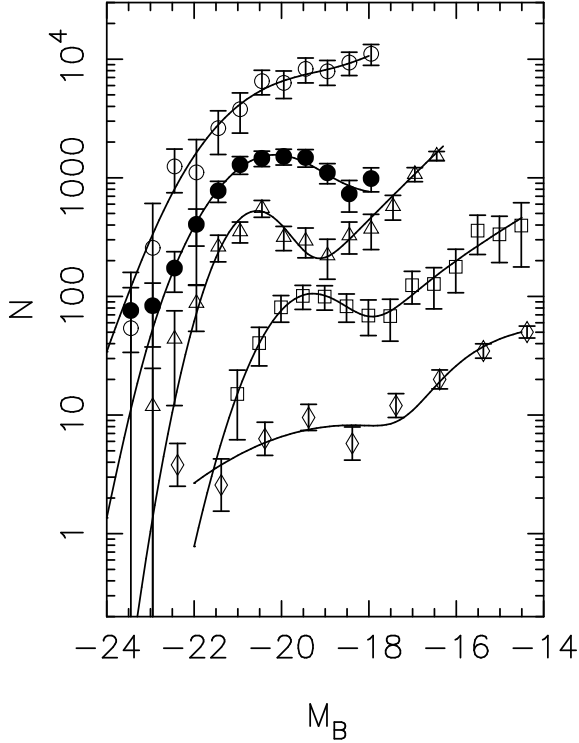


**Figure 6.** Luminosity function in the rest-frame  $B$ -band for Cl1601+42 at  $z = 0.54$  (open circles), Cl0016+16 at  $z = 0.55$  (filled circles), MS1008–1224 at  $z = 0.31$  (triangles), Coma at  $z = 0.02$  (squares) and Virgo at  $z = 0.003$  (diamonds). Data for Coma and Virgo are taken from Trentham (1998a) and Trentham & Hodgkin (2002), respectively. The LFs are arbitrary off-set in the  $y$ -direction.

different clusters, but with varying relative strengths. This suggests an universality for type-specific LFs. This is analogous to the claim of type-specific LFs for different morphological types by Binggeli et al. (1988) and Andreon (1998). A comparison with Binggeli et al. (1988) is especially interesting, since they find that the bright part of the LF mainly consists of elliptical galaxies with a Gaussian LF, and that the steep faint-end consists of irregulars and dEs. This suggests, as expected, that the early-type population mainly consists of ellipticals, while many faint late-type galaxies are irregulars. To explain the different shapes of the high- $z$  cluster LFs, we argue that these reflect different dynamical states of the clusters. As the clusters get dynamically older, we expect the late-type population to fade relative to the early-type population, and LFs to become more similar.

## 5.2 The dwarf population in MS1008–1224

The faint limit in absolute magnitude we reach for MS1008–1224 at  $z = 0.31$  allows us to study the dwarf population  $\sim 1.5$  mag deeper in this cluster compared to the clusters at  $z \sim 0.55$ . Studies by Trentham (1998c) and Boyce et al. (2001) have shown that dwarf irregular (dIrr) galaxies have  $B - R \sim 0.9$ , while dEs have colours in a broader range  $1.3 \lesssim B - R \lesssim 2.0$ . To compare the colours of the dwarf population in MS1008–1224 with other nearby clusters, with more limited colour information, we therefore

plot in Fig. 7 the rest-frame  $B - R$  colours of galaxies with  $-17.7 < M_B < -16.2$ .

In the  $B - R$  histogram of MS1008–1224 in Fig. 7 there are two peaks, suggesting that there indeed are two distinct populations representing dIrrs and dEs. In the figure we also show the distribution of  $B - R$  colours for the faint galaxies, which on the basis of the full  $BVRI$  photometry we have classified as early-type and late-type galaxies, respectively. The fact that this classification closely follows the two-colour division into the two peaks shows that we reliably can use the  $B - R$  colour to broadly distinguish between early-type and late-type galaxies.

From the  $B - R$  colours Trentham (1998c) finds that all dwarf galaxies with  $-18.9 < M_R < -16.9$  in Abell 665 at  $z = 0.18$  are consistent with being dEs (called dSphs by Trentham). In Abell 963 at  $z = 0.21$  the majority of the dwarf galaxies with  $-19.2 < M_R < -18.2$  also have colours consistent with dEs. There is, however, in this cluster also a population with colours intermediate between dEs and dIrrs, which Trentham proposes may represent a transitional stage between these types.

In a recent study Boyce et al. (2001) investigate the  $B - R$  colour of galaxies with  $-19 < M_R < -16.5$  in Abell 868 at  $z = 0.154$ . They find a distribution in colour with two peaks, showing the presence of a dominant population of dEs, but also a population of dIrrs. For the faintest galaxies ( $-17.5 < M_R < -16.5$ ) there are similar numbers of dEs and dIrrs.

The main difference between MS1008–1224 and lower-redshift clusters is the relative fraction of dIrrs to dEs. To make a quantitative comparison between the faint populations, we use the  $B - R$  index to calculate the fraction of dIrrs for MS1008–1224, Abell 963, Abell 665 and Abell 868. We assume that galaxies with rest-frame  $B - R < 1.2$  are dIrrs, which is the criterion used by Boyce et al. (2001).

A complication is that MS1008–1224 is not observed in standard Johnson–Cousins filters, but in Bessel filters. To correct for this we use galaxy templates from Coleman et al. (1980) and filter transmission curves to calculate the transformation between the standard  $B - R$  colours and the  $B - R$  colours for the Bessel filters. We then find that the division between dIrrs and dEs at  $B - R = 1.2$  in standard Johnson–Cousins filters corresponds to  $B - R = 1.34$  in the Bessel filters.

Using this criterion, we find that the fraction of faint galaxies that belong to the dIrr population is  $0.72 \pm 0.03$  for MS1008–1224, to be compared with  $0.07 \pm 0.03$  for Abell 963,  $0.01 \pm 0.01$  for Abell 665 and  $0.22 \pm 0.02$  for Abell 868. A further problem when comparing these numbers is that the different investigations use different magnitude intervals for defining the dwarf populations. Irrespective of this, however, we reach the important conclusion that MS1008–1224 is dominated by dIrrs, while the lower redshift clusters are dominated by dEs.

The fraction of dIrrs in Coma, classified by the same colour criterion as above, for galaxies with  $-15.3 < M_R < -13.3$  is  $0.11 \pm 0.01$  (calculated from fig. 7 in Trentham 1998a). The fraction of *morphological* dIrrs in Virgo ( $-17.8 < M_B < -15.8$ ), calculated from fig. 6 in Trentham & Hodgkin (2002), is  $0.25 \pm 0.07$ . The results emphasize the conclusion that dEs dominate the faint population in nearby clusters, while our study shows that the

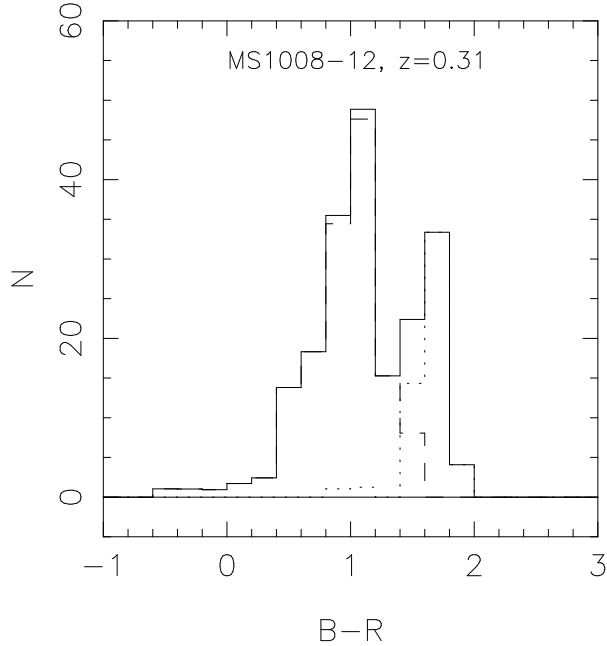


**Figure 7.** The rest-frame  $B-R$  colour distribution for galaxies in MS1008-1224 with  $-17.7 < M_B < -16.2$ . The solid line shows the total number of galaxies, while the dotted and dashed lines show the distribution of early-type and late-type populations, as classified by multi-band photometry, separately.

opposite is true for MS1008-1224 at  $z = 0.31$ . It would obviously be of great interest to study more clusters to these limits to see if this is a general property.

Galaxy harassment could here be a mechanism that transforms the faint late-type population, dominating medium redshift clusters such as MS1008-1224, into dEs, as shown by Conselice et al. (2001). The similarity between the faint-end slopes of the late-type population ( $\alpha_f = -1.84 \pm 0.12$ ) and the early-type population ( $\alpha_f = -1.69 \pm 0.14$ ) at faint magnitudes ( $M_B > -19$ ) is consistent with this picture. Based on these observations alone, we cannot, however, rule out that slower mechanisms such as 'strangulation' (Balogh et al. 2000), are at least partly responsible for the luminosity and colour evolution.

### 5.3 Dwarf-to-giant ratio

Previous studies have shown that the ratio of faint to bright galaxies increases at large radii, where the surface density decreases. Driver et al. (1998) find that five out of seven clusters at  $z \sim 0.15$  show an increasing dwarf-to-giant ratio with radius. A  $K$ -band study of AC 118 at  $z = 0.3$  by Andreon (2001) shows the same trend. In DFN02 we found that Cl1601+42 has a steeper faint-end slope of the LF in the outer part of the cluster, which is equivalent to an increasing dwarf-to-giant ratio.

Here, we calculate the dwarf-to-giant ratio by defining galaxies with  $-19.5 < M_B < -17.7$  as dwarfs, and brighter galaxies as giants. The separation between dwarfs and giants is chosen to match the cross-over in the cluster LFs between early-type and late-type galaxies (Fig. 5). This division is somewhat brighter than used in other papers (e.g., Driver et al. 1998), and is here adopted in order to get

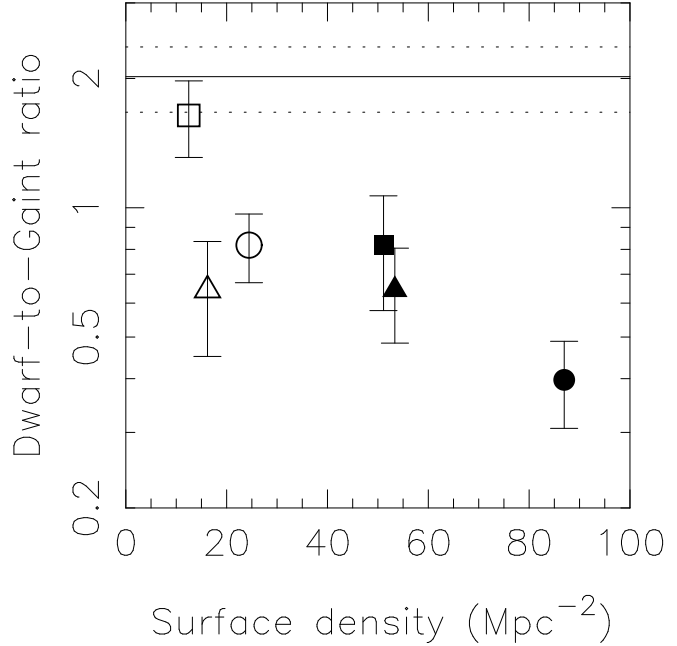


**Figure 8.** Dwarf-to-giant ratio as a function of bright galaxy surface density for Cl0016+16 (circles), Cl1601+42 (squares) and MS1008-1224 (triangles). Filled symbols represent the inner region of the cluster ( $R < 0.5$  Mpc), while open symbols represent the outer region. The horizontal lines represent the field value (solid line) and  $1\sigma$ -errors (dotted lines).

sufficient statistics in the faint bin. We further divide each cluster into a core region with projected radius  $< 0.5$  Mpc, and an outer region between 0.5 and 1.1–1.5 Mpc, depending on cluster.

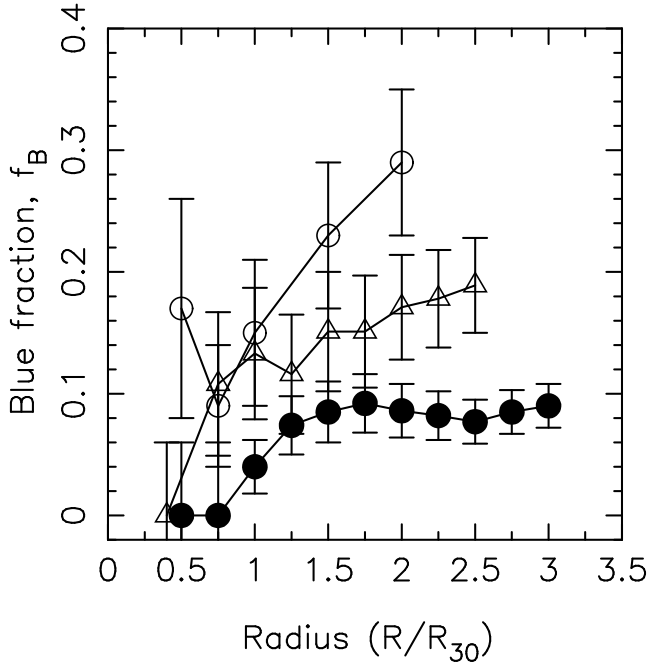
In Fig. 8 we plot the resulting dwarf-to-giant ratios as function of surface density of the giant galaxies for these two regions in all clusters. Cl0016+16 is represented by circles, Cl1601+42 by squares and MS1008-1224 by triangles. Filled symbols show results for the core area, while open symbols represent results from the outer area. The horizontal lines represent the field value and the corresponding  $1\sigma$ -errors.

Fig. 8 shows that Cl0016+16 and Cl1601+42 have a clear trend of an increasing dwarf-to-giant ratio when going from the inner high-density region, to the outer lower-density region, which is consistent with the trend found by Phillipps et al. (1998) and with Andreon (2001). As an explanation of this these authors suggest that the high-density environment in cores of clusters is hostile to the dwarf galaxies, while the outer, low-density regions do not affect this population, which therefore have a dwarf-to-giant ratio and faint-end slope similar to that of the field.

For the low redshift cluster MS1008-1224, there is no obvious trend. We note, however, that the error in the dwarf-to-giant ratio is substantial.

### 5.4 The Butcher–Oemler effect as function of radius and limiting magnitude

The BO effect is of major observational importance as a probe of the cluster galaxy population. Although much of the discussion below to a large extent is a consequence of the early-type and late-type LFs in Fig. 5 and their dependence



**Figure 9.** The blue fraction,  $f_B$ , as a function of radius for Cl0016+16 (filled circles), Cl1601+42 (open circles) and MS1008–1224 (triangles).  $R_{30}$  is the fiducial value used by BO84 for calculating  $f_B$ .

on radius (e.g., Fig. 3), we will for this reason illustrate the consequences of this with two important implications for the BO effect.

Already in BO84, and more recently in DFN02, it was pointed out that the blue fraction  $f_B$  increases at larger radii. This can be understood as a result of the fact that early-types are in general more centrally concentrated than late-types. In Fig. 9 we show the dependence of  $f_B$  on radius, where the radius is given in fractions of  $R_{30}$  (as defined in Section 4.3). Also in this respect Cl0016+16 deviates from the other clusters. Inside of  $1.25R_{30}$ ,  $f_B$  decreases rapidly, while outside this radius  $f_B$  stays almost constant, at a value well below that of the other clusters. Cl1601+42 on the other hand shows a steep radial dependence. The higher blue fraction in Cl1601+42 is consistent with the higher fraction of late type galaxies in this cluster (Fig. 3). MS1008–1224 has a trend in between the two higher redshift clusters. From a very low  $f_B$  in the core region, there is a rapid increase to  $\sim 1.25 R_{30}$ , followed by a slower increase in the outer regions. The behaviour of  $f_B$  in these clusters reflects, as expected, the radial dependence of the early-type fraction shown in the right panel of Fig. 3.

In DFN02 we showed that  $f_B$  in Cl1601+42 depends strongly of the limiting magnitude. This dependence is a direct consequence of the different shapes of the early-type and late-type LFs in this cluster. At fainter magnitudes the total LF becomes more dominated by late-type galaxies, which leads to a higher  $f_B$ . In Fig. 10 we plot the dependence of  $f_B$  on the limiting magnitude for the three clusters. As expected, the increase of  $f_B$  is much weaker in Cl0016+16 than in Cl1601+42, which is consistent with the LF for this cluster being dominated by early-type galaxies to fainter magnitudes (Fig. 5). MS1008–1224 again shows an intermediate

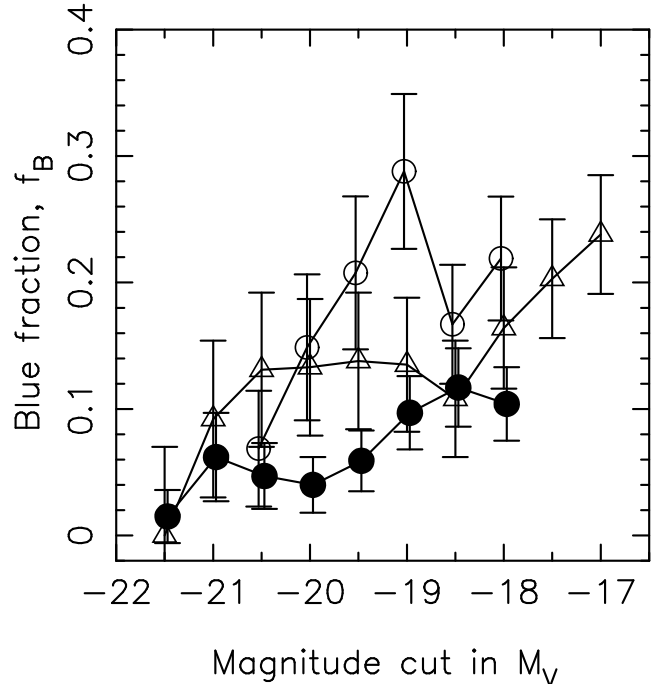


**Figure 10.** The fraction of blue galaxies,  $f_B$ , as a function of limiting magnitude for Cl0016+16 (filled circles), Cl1601+42 (open circles) and MS1008–1224 (triangles).

behaviour. The strong increase in  $f_B$  at faint magnitudes in MS1008–1224 is caused by the dominating population of blue dwarf galaxies.

## 6 SUMMARY

This work represents one of the deepest studies of the LF for intermediate-redshift clusters, several magnitudes beyond  $L^*$ . In addition, we have demonstrated the usefulness of photometric redshifts for selecting clusters members, as well as for population studies of distant clusters of galaxies. As a result, while most previous determinations of distant cluster LFs have treated only the *total* LF, we have in this study been able to separate the early-type and late-type populations. This has been possible, despite the moderate telescope size due exactly to the use of photometric redshifts. Compared to the usual subtraction method, we have been gaining a large factor in respect to the background contamination.

Our main conclusions from this study are:

- There is no universal shape of the *total* cluster LF at  $z \gtrsim 0.3$ .
- The early-type population has a Gaussian LF, while the late-type population is well fitted by a Schechter function. This suggests that the LFs for different spectral populations could be universal, while the total LF depends on the relative abundance of these populations.
- The evolution of the late-type galaxies is consistent with a fading by  $\sim 2$  magnitudes between  $z \sim 0.55$  and  $z = 0$ , while the early-type population fades by  $\sim 1$  mag. This scenario suggests that the total LFs of the high- $z$  clusters become more similar to local LFs as the clusters get dynamically older.

- The red cluster Cl0016+16 is an atypical high- $z$  cluster that resembles local rich clusters in many aspects, indicating an old dynamical age despite its redshift. It does, however, contain a large fraction of post-starburst galaxies, suggesting that star formation was more intense at  $z \gtrsim 0.8$ , and that the infall was very low during the last  $\sim 1$  Gyr before the cluster is observed.
- In MS1008–1224 at  $z = 0.31$ , we find that dIrrs dominate over dEs, opposite to what is found in nearby clusters. If this is confirmed for more clusters at this redshift it implies a dramatic evolution of the dwarf population.
- The relation between dwarf-to-giant ratio and surface density indicates that high-density regions are hostile to dwarfs, consistent with a destruction or fading of this population by galaxy harassment.
- We find that the blue fraction,  $f_B$ , as defined by BO84 varies with radius and limiting magnitude. This is a direct consequence of the radial gradient of the late-type galaxies and the relative normalisation of the late-type and early-type LFs.

There are several natural next steps to this study. The sample needs to be expanded, both in terms of redshift and cluster properties. As the example of Cl 0016+16 has shown, even at the same redshift the the population may vary greatly, depending on the dynamical state, and possibly on the environment. A better understanding of this is of obvious importance for the understanding of the cluster-formation process, especially at redshifts higher than we have probed.

Spectroscopic studies at redshifts similar to the clusters in this study may today marginally be carried out with 8–10 m class telescopes. This would of course give more detailed information about the dynamical properties of the clusters, as well as a general check of the reliability of the photometric redshift method for clusters. At higher redshifts it is, however, virtually impossible to probe the population beyond  $L_*$  with spectroscopy, even with these telescopes. For this type of investigations one therefore has to rely on photometric redshifts, in this case extended to include the near-infrared bands. The study in this paper, as well as DFN02, hopefully represents some first steps in this direction.

Also at low redshifts there are several open questions, especially connected to the dwarf population. The dramatic difference in the dIrr-to-dSph ratio seen between MS1008–1224 and the local clusters needs to be confirmed with more medium-redshift clusters.

Finally, our study has mainly given information about the broad band colours of the cluster members. A high-resolution study with HST of the morphological properties of these galaxies would be of prime interest, as was partially demonstrated for Cl 1601+42 in DFN02, and in more detail for the bright population by e.g. the MORPHS sample (Smail et al. 1997). We hope in the future to pursue some of these questions.

## ACKNOWLEDGMENTS

We are grateful to Neil Trentham and Claes-Ingvar Björnsson for several useful comments and to the referee for many valuable comments and suggestions. Nordic Optical Telescope is operated on the island of La Palma jointly

by Denmark, Finland, Iceland, Norway, and Sweden, in the Spanish Observatorio del Roque de los Muchachos of the Instituto de Astrofísica de Canarias.

The data presented here have been taken using ALFOSC, which is owned by the Instituto de Astrofísica de Andalucía (IAA) and operated at the Nordic Optical Telescope under agreement between IAA and the NBIfAFG of the Astronomical Observatory of Copenhagen.

This paper is also based on observations obtained at the Very Large Telescope at Cerro Paranal operated by the European Southern Observatory.

This work has been supported by the Swedish Research Council.

## REFERENCES

Andreon S., 1998, A&A, 336, 98  
 Andreon S., 2001, ApJ, 547, 623  
 Balogh M.L., Navarro J.F., Morris S.L. 2000, ApJ, 540, 113  
 Baugh C.M., Cole S., Frenk C.S. 1996, MNRAS, 282, L27  
 Benítez N., 2000, ApJ, 536, 571  
 Binggeli B., Sandage A., Tammann G.A., 1988, ARA&A, 26, 509  
 Bower R.G., 1991, MNRAS, 248, 332  
 Bower R.G., Kodama T., Terlevich, A., 1998, MNRAS, 299, 1193  
 Boyce P.J., Phillipps S., Jones J.B., Driver S.P., Smith R.M., Couch W.J. 2001, MNRAS, 328, 277  
 Brunner R.J., Lubin L.M., 2000, AJ, 120, 2851  
 Bruzual G., Charlot S., 2003, MNRAS, 344, 1000  
 Butcher H., Oemler A., 1984, ApJ, 285, 426 (BO84)  
 Carlberg R.G., Yee H.K.C., Ellingson E., Abraham R., Gravel P., Morris S., Pritchett C.J. 1996, ApJ, 462, 32  
 Coleman G.D., Wu C.-C., Weedman D.W., 1980, ApJS, 43, 393  
 Connolly A.J., Szalay A.S., Koo D., Romer A.K., Holden B., Nichol R.C., Miyaji T., 1996, ApJ, 473, 67  
 Conselice C.J., Gallagher J.S., Wyse R.F.G., 2001, ApJ, 559, 791  
 da Costa, L.N., et al., 1998, submitted to A&A, (astro-ph/9812105), under revision and update  
 Dahlén T., Fransson C., Näslund M. 2002, MNRAS, 330, 167 (DFN02)  
 De Propris R., Stanford S.A., Eisenhardt P.R., Dickinson M., Elston R., 1999, AJ, 118, 719  
 Diaferio A., Kauffmann G., Balogh M.L., White S.D.M., Schade D., Ellingson E. 2001, MNRAS, 323, 999  
 Dressler A., Gunn J.E. 1992, ApJS, 78, 1  
 Dressler A., Smail I., Poggianti B.M., Butcher H., Couch W.J., Ellis R.S., Oemler A., 1999, ApJS, 122, 51  
 Driver S.P., Phillipps S., Davies J.I., Morgan I., Disney M.J., 1994, MNRAS, 268, 393  
 Driver S.P., Couch W.J., Phillipps S., 1998, MNRAS, 301, 369  
 Dubinski J., 1998, ApJ, 502, 141  
 Ellingson E., Lin H., Yee H.K.C., Carlberg R.G., 2001, ApJ, 547, 609  
 Ferguson H.C., Sandage A., 1991, AJ, 101, 765  
 Gioia I.M., Luppino G.A., 1994, ApJS, 94, 583  
 Gunn J.E., Stryker L.L., 1983, ApJS, 52, 121  
 Henry J.P., Soltan A., Briel U., Gunn J.E. 1982, ApJ, 262, 1  
 Hughes J.P., Birkinshaw M. 1998, ApJ, 497, 645  
 Jarvis J.F., Tyson J.A., 1981, AJ, 86, 476  
 Kauffmann G., 1995, MNRAS, 274, 153  
 Kauffmann G., White S.D.M., Guiderdoni B., 1993, MNRAS, 264, 201  
 Kodama T., Bower R.G., 2001, MNRAS, 321, 18  
 Kodama T., Bell E.F., Bower R.G., 1999, MNRAS, 302, 152  
 Koo D.C., 1981, ApJ, 251, L75  
 Landolt A.U., 1992, AJ, 104, 340

Lewis A.D., Ellingson E., Morris S.L., Carlberg R.G., 1999, *ApJ*, 517, 587

Liu C.T., Green R.F., 1998, *AJ*, 116, 1074

Madau P., 1995, *ApJ*, 441, 18

Margoniner V.E., de Carvalho R.R., Gal R.R., Djorgovski S.G., 2001, *ApJ*, 548, 143

Moore B., Lake G., Katz N., 1998, *ApJ*, 495, 139

Näslund M., Fransson C., Huldtgren M. 2000, *A&A*, 356, 435

Oke J.B., Gunn J.E., Hoessel J.G., 1996, *AJ*, 111, 29

Phillipps S., Driver S.P., Couch W.J., Smith R.M., 1998, *ApJ*, 498, L119

Poggianti B.M., Smail I., Dressler A., Couch W.J., Berger A.J., Butcher H., Ellis R.S., Oemler A., 1999, *ApJ*, 518, 576

Postman M., Lauer T.R. 1995, *ApJ*, 440, 28

Rakos K.D., Schombert J.M., 1995, *ApJ*, 439, 47

Sandage A., 1976, *ApJ*, 205, 6

Schlegel D.J., Finkbeiner D.P., Davis M. 1998, *ApJ*, 500, 525

Schechter P., 1976, *ApJ*, 203, 297

Smail I., Ellis R.S., Fitchett M.J., Edge A.C., 1995, *MNRAS*, 273, 277

Smail I., Dressler A., Couch W.J., Ellis R.S., Oemler A., Butcher H., Sharples R.M., 1997, *ApJS*, 110, 213

Smail I., Edge A.C., Ellis R.S., Blandford R.D., 1998, *MNRAS*, 293, 124

Smith R.M., Driver S.P., Phillipps S., 1997, *MNRAS*, 287, 415

Trentham N., 1998a, *MNRAS*, 293, 71

Trentham N., 1998b, *MNRAS*, 294, 193

Trentham N., 1998c, *MNRAS*, 295, 360

Trentham N., Hodgkin S., 2002, *MNRAS*, 333, 423

Valdes F., 1982, Faint Object Classification and Analysis System. NOAO, Tucson, AZ

Valdes F., 1993, FOCAS User's Guide. NOAO, Tucson, AZ

van Dokkum P.G., Franx M., Fabricant D., Kelson D.D., Illingworth G.D., 1999, *ApJ*, 520, L95

Wilson G., Smail I., Ellis R.S., Couch W.J., 1997, *MNRAS*, 284, 915

Yagi M., Kashikawa N., Sekiguchi M., Doi M., Yasuda N., Shimasaki K., Okamura S., 2002, *AJ*, 123, 87

Yee H.K.C., Ellingson E., Morris S.L., Abraham R.G., Carlberg R.G., 1998, *ApJS*, 116, 211